European Polymer Journal 119 (2019) 1–7

Contents lists available at ScienceDirect

European Polymer Journal

journal homepage: www.elsevier.com/locate/europolj

Mechanical, thermal, and morphological properties of natural rubber/45S5 Bioglass® fibrous mat with ribbon-like morphology produced by solution blow spinning

Eliraldrin Amorin Sousa[a], Michael Jones Silva[b,*], Alex Otávio Sanches[a], Viviane Oliveira Soares[c], Aldo Eloizo Job[d], José Antonio Malmonge[a]

[a] Universidade Estadual Paulista (UNESP), Faculdade de Engenharia, Câmpus de Ilha Solteira, Avenida Brasil, 56, Centro, 15385-000, Ilha Solteira, São Paulo, Brazil
[b] Universidade Estadual Paulista (UNESP), Câmpus Experimental de Rosana, Avenida dos Barrageiros, 1.881, Centro, 19.274-000, Rosana, São Paulo, Brazil
[c] Universidade Estadual de Maringá (UEM), Câmpus Regional de Goioerê, Avenida Reitor Zeferino Vaz, s/n - Jardim Universitário, 87360-000, Goioerê, Paraná, Brazil
[d] Universidade Estadual Paulista (UNESP), Faculdade de Ciências e Tecnologia, Campus de Presidente Prudente, Rua Roberto Simonsen, 305, Centro Educacional, 19060-900, Presidente Prudente, São Paulo, Brazil

ARTICLE INFO

Keywords:
Solution blow spinning
Natural rubber
45S5 Bioglass®
Fibrous mats biocomposite

ABSTRACT

Natural rubber (NR)/45S5 Bioglass® (BG) based fibrous mat biocomposite were fabricated using a solution blow spinning (SBS) method. NG/BG fibrous mat with ribbon-like morphology were obtained with different amounts of 45S5 BG to NR. Biocomposites exhibited uniform diameter distribution of fibers in the 40–60 μm range. The preparation method and dispersion of particles in the NR matrix had significant influence on the final mechanical properties of the biocomposite, i.e., the tensile strength of membrane samples increased, while the elongation decreased compared to those of neat NR films. The glass transition temperature (T_g) value of the biocomposite samples shifted toward higher temperatures due to the movement restriction of the NR chains caused by the BG particles. For the biocomposite samples T_g was in the range of −30 to −28 °C, whereas for the NR film and NR fibrous mat T_g was −46.7 and −40.5 °C respectively. The Cole-Cole plot was an imperfect semicircle indicating the heterogeneity of the system as well as the adequate interaction between BG and NR. The production of membrane biocomposites with good thermal and mechanical properties employing the SBS method could be promising and potential for biomedical applications.

1. Introduction

Biomaterials are synthetic or natural substances or combinations of these substances, that can be used for any period of time, and that augment or partially or totally replace any tissue, organ, or function of the body, while maintaining or improving the quality of life of the individual [1,2]. The biomaterials that stand out the most are metal alloys, polymers, and glass-ceramic materials. Among glass-ceramic materials, bioglasses are particularly important, and have been widely used in medicine [3]. One of the most studied bioactive glasses is 45S5 Bioglass®, which has been known as the bioactive glass with the highest bioactivity index (I_B = 12.5) and is still considered the gold standard of bioactive materials [4]. Hench first introduced 45S5 BG in the early 1970s, and since then it has been used in several biomedical applications [5]. The chemical composition of 45S5 BG, which is a silica-based melt-derived glass, is as follows: 24.5 Na_2O–24.5 CaO–45 SiO_2–6 P_2O_5 (wt.%). When BG comes in contact with bodily fluids it forms a hydroxycarbonate apatite (HCA) layer on its surface, which is chemically and structurally similar to the mineral apatite phase found in bone tissues. Moreover, BG presents osteoconductive and osteoinductive properties which allow for its applications in repairing damaged bones and teeth, and as remineralizing agent [6,7]. However, despite its excellent bioactive properties, BG presents low mechanical strength and low fracture toughness, which restrict its applications for situations that involve mechanical stresses and conformability [8,9]. To improve the mechanical properties and/or expand the range of medical applications, biocomposites can be developed based on polymeric matrices [10–12]. Of all synthetic and natural polymers, natural rubber deserves a special mention owing to its unique mechanical proprieties and biocompatibility. Extracted as latex from *Hevea brasiliensis,* NR is a biopolymer with high molecular weight consisting of isoprene units linked in *cis*-1,4 conformation. Its main characteristics are its elasticity, flexibility,

* Corresponding author.
E-mail address: michael.silva@unesp.br (M.J. Silva).

https://doi.org/10.1016/j.eurpolymj.2019.07.002
Received 4 February 2019; Received in revised form 30 June 2019; Accepted 1 July 2019
Available online 02 July 2019

resilience, and excellent mechanical resistance [13]. Due to its excellent biocompatibility with living tissues, as well as its high angiogenic potential NR is an important material in biomedicine [14,15].

Different techniques have been developed in the search for different biocomposite morphologies for biomedical applications: electrospinning [16–18], casting [19], extrusion [20], solution blow spinning (SBS) [21,22], etc. Among these techniques, SBS is an alternative method to produce polymeric fibers, which can substitute the well-established electrospinning method [23]. The main advantage of SBS is its higher rate of fiber production (measured by the injection of solution) compared to electrospinning. Moreover, SBS involves low production costs, is easy to implement, and does not require the use of high electric fields, which allows the deposition of fibers on any type of target [24]. The potential of using the SBS technique to develop highly porous bioactive fibers for tissue engineering has been investigated by Medeiros et al. [25]. The authors obtained fibers composed of poly(D,L-lactide) and dimethyl carbonate in a cryogenic environment and were subsequently lyophilized, which generated three-dimensional (3D) scaffolds consisting of porous nanofibers featuring interconnected macropores [25].

In one of our previous studies, we fabricated biocomposites consisting of NR fibers and 45S5 BG particles using the casting/evaporation method, and investigated their morphology, mechanical, and thermal properties [11]. In this study, we used the SBS technique to fabricate fibrous mat of NR microfibers and 45S5 BG particles, and investigated their mechanical and thermal properties. The fibrous mat exhibited "ribbon-like" morphology, and their mechanical properties were superior to those of NR cast films. The fibrous mat obtained by incorporating up to 50% m/m BG into the NR matrix maintained their ribbon-like morphology, malleability, and elasticity.

2. Material and methods

2.1. Natural rubber

We collected NR latex from *Hevea brasiliensis* trees (Rubber Research Institute of Malaysia (RRIM) 600 Clone) in the experimental farm of the São Paulo State University (UNESP), Ilha Solteira campus, Brazil. After extraction, NR latex was filtered and stored in an appropriate place without the use of preservatives. Subsequently, NR films were produced using the casting method and dried in an oven at 60 °C for 24 h.

2.2. 45S5 Bioglass® particles preparation

We prepared 45S5 BG (composition: 24.5 Na_2O–24.5 CaO–45 SiO_2–6 P_2O_5 (wt.%)) using the following reagent grade chemicals: sodium carbonate (Na_2CO_3, JT Baker, USA), calcium carbonate ($CaCO_3$, JT Baker, USA), disodium hydrogen phosphate (Na_2HPO_4, JT Baker, USA), and high-purity quartz powder (SiO_2, Santa Rosa, Brazil). The analytical reagents were weighed and homogenized using a jar mill at 150 rpm for 1 h. We melted 100 g 45S5 BG in an electric furnace (Deltech Corp., USA) at 1450 °C for 4 h, using a Pt crucible. The melt was poured on a stainless-steel platform and pressed using a stainless-steel plaque. The obtained glass pieces were not annealed to avoid the premature formation of crystalline nuclei, and they were first ground in an agate mortar to obtain large particles (~2 mm). These particles were then milled in a high impact planetary ball mill (Pulverisette 5, Fritsch) at 450 rpm for 90 min using an agate jar and 20 mm diameter agate balls.

2.3. Preparation of polymer solution and composite dispersions for SBS

The methodology described by Silva et al. [11] was employed to obtain NR/BG fibrous mat biocomposites. A 4% m/v NR solution was prepared by dissolving a small piece of NR film in chloroform under magnetic stirring for 12 h. Then, BG particles were added to the NR solution under constant stirring for 1 h to ensure the good dispersion of the biocomposites. To produce fibrous mat, 3 mL NR solution or biocomposite dispersion was first drawn into a disposable syringe (using a 20G spinal needle) coupled to an injection system.

The most optimal conditions for the formation of the microfiber were determined to be as follows: gas (filtered air) pressure of 400 kPa, injection rate of 263 μL min^{-1}, work distance of 15 cm. Moreover, the angular velocity and diameter of the collector, which was wrapped in aluminum foil, were 50 rpm and 10 cm, respectively. These conditions were maintained for all experiments. The mass ratios and the viscosity (Brookfield Thermosel system with a rotational DV-II + (model LVDV-II) viscometer) of NR/BG used in this study were 100/00 (3.8 Pa s) , 90/10 (5.2 Pa s), 70/30 (5.8 Pa s), and 50/50 (6.3 Pa s).

2.4. Characterization

A scanning electron microscope (SEM, EVO LS15 Zeiss) was employed to observe the surface morphologies of the samples. All samples were previously coated with carbon by sputtering for 30 min. Thermogravimetric (TG) analysis was performed using a Q 600 TA Instruments device in the 25–600 °C temperature range, at a heating rate of 10 °C min^{-1} in a nitrogen atmosphere with a flow rate of 100 mL min^{-1}. Approximately 10 mg of each sample for TG analysis was used. Dynamic mechanical thermal analysis (DMTA) measurements were performed during tension cycled on rectangular specimens approximately 9 mm × 3 mm × 1 mm in size using a Netzsch model DMTA 242C instrument in tensile mode. The parameters used were as follows: frequency of 10 Hz, temperature range from −100 to 150 °C and heating rate of 5 °C min^{-1}, amplitude of 240 μm, and maximum dynamic force of 1.6 N. The storage modulus (E'), loss modulus (E''), and tan δ (ratio between E' and E'') were obtained from the DMTA measurements. Mechanical tests (stress-strain mode) were performed on the samples at room temperature using an Instron universal testing machine (model 3639) in accordance with ISO 37:2011 standard using a load cell of 500 N and crosshead speed of 500 mm min^{-1}. according to ISO 1286:2006. The samples were cut according to ISO 1286:2006, and the results were averaged from eighth test.

3. Results and discussion

3.1. Optical analysis

Fig. 1 illustrates the obtained 50/50 NR/BG fibrous mat biocomposite. Fig. 1a depicts a photograph of the biocomposite stretched to approximately 2.5 times its original size, thus illustrating its flexibility and good mechanical properties. Fig. 1b shows the optical micrograph of the same sample, where its fibrous morphology and BG particles (white dots), which are regularly distributed along the microfibers, can be observed.

3.2. Morphology

Fig. 2a–f shows SEM images of the BG particles, NR fibrous mat, and NR/BG fibrous mat biocomposites. The BG particles exhibited irregular morphology with an average particle size of 6 ± 3 μm, as shown in Fig. 2a. Both the NR fibrous mat and fibrous mat biocomposites exhibited ribbon-like morphology, unlike the cylindrical structures commonly observed in films produced by SBS using other polymers [26]. As reported by Koombhongse et al. [27], a variety of structures, such as microfibers, beads, and ribbons can be obtained using the electrospinning technique. The sizes and shapes of these structures are governed by a number of variables, such as the polymer solution properties, vapor pressure of solvent, and humidity, as well as process parameters, such as the injection rate and electrical field strength [28–30]. The flat microfibers obtained in our study could be the result of cylindrical microfibers collapsing owing to the high amount of internal solvent.

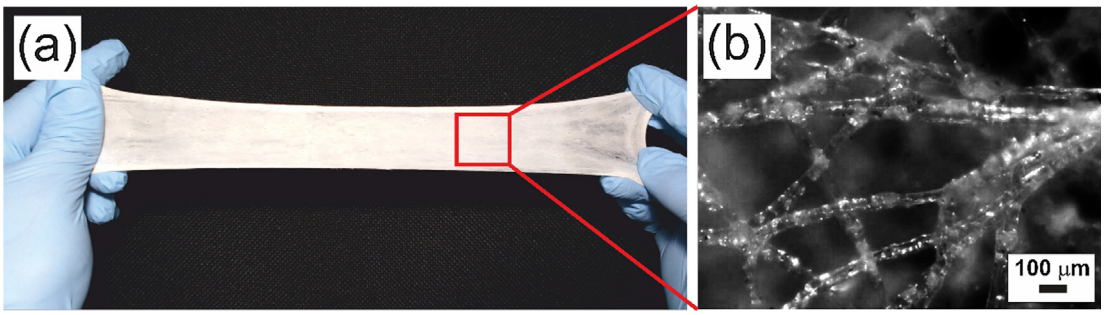

Fig. 1. (a) Stretched and (b) optical micrograph of 50/50 NR/BG fibrous mat.

Microfibers dry from the outside to the inside; as a result, the encapsulated solution tends to migrate to the edge region due to centrifugal forces from the collector and subsequently collapses, forming flat microfibers (Fig. 2c).

Fig. 2 also illustrates the presence of BG particles encapsulated by NR as well as the BG particles on the surface of NR microfibers. The addition of BG particles resulted in the formation of defects (BG particles in the microfiber surface), which increased the roughness of the microfibers. The microfibers width distributions are presented in the insets of Fig. 2 for each sample, and the average widths of the microfibers were similar, ranging from 44 ± 12 to 60 ± 12 μm.

3.3. Mechanical analysis

Fig. 3 shows the mechanical behavior of the NR film obtained by casting compared to the NR fibrous mat and NR/BG fibrous mat biocomposites obtained by SBS. The NR film displayed behavior typical of elastomeric polymers exhibiting elongation at break of 700 ± 45% as shown in Table 1. On the other hand, the NR fibrous mat presented a reduction in deformation compared to the NR film, exhibiting a deformation of 384 ± 24%. However, the Young modulus (Y) and tensile strength at break ($\sigma_{at\ break}$) of the NR fibrous mat (6.12 ± 0.09 MPa and 1.62 ± 0.12 MPa, respectively), were approximately 1742 and 165%,

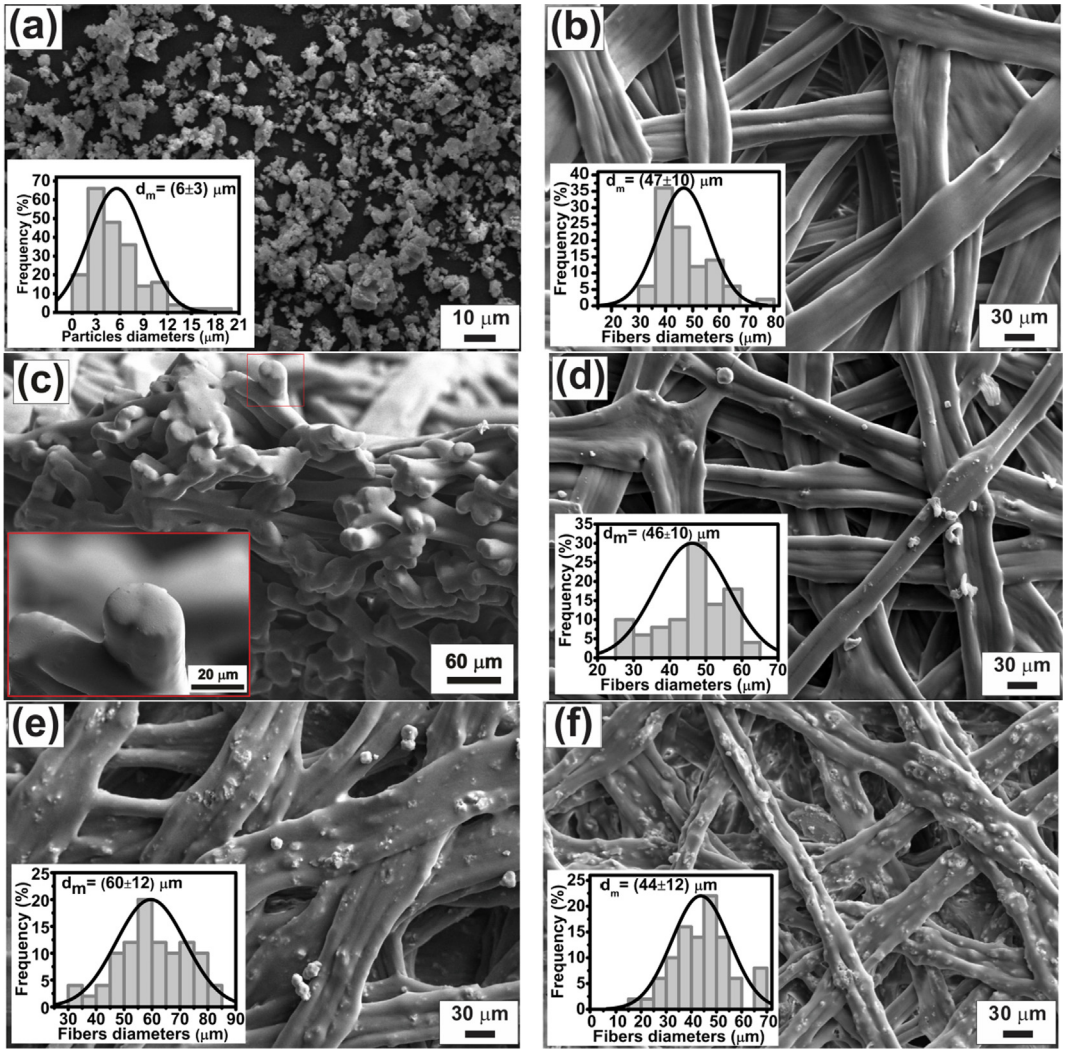

Fig. 2. SEM images and average diameter (d_m) diagram of the (a) BG particles, (b) NR fibrous, (c) cross-section fracture of the NR fibrous, (d) 90/10, (e) 70/30 and (f) 50/50 NR/BG fibrous mats biocomposite.

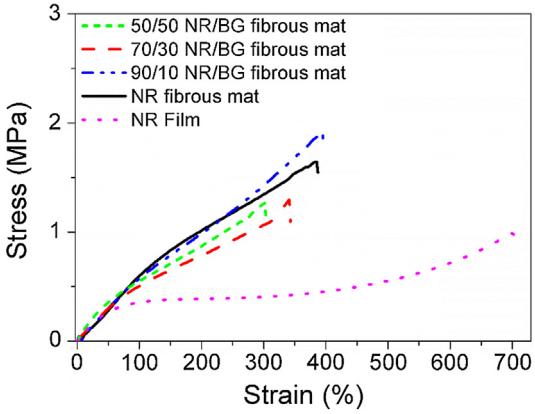

Fig. 3. Stress-strain tests of the NR film, NR fibrous mat, and NR/BG fibrous mats biocomposite containing various BG loading amounts.

Table 1
Elongation at break ($\varepsilon_{at\ break}$), tensile strength at break ($\sigma_{at\ break}$), and Young modulus (Y) of the samples.

Sample	*Y* (MPa)	$\sigma_{at\ break}$ (MPa)	$\varepsilon_{at\ break}$ (%)
NR film	0.35 ± 0.05	0.98 ± 0.02	700 ± 45
NR fibrous mat	6.1 ± 0.9	1.62 ± 0.12	384 ± 24
90/10 NR/BG fibrous mat	5.8 ± 0.6	1.91 ± 0.07	392 ± 6
70/30 NR/BG fibrous mat	5.0 ± 0.3	1.18 ± 0.16	337 ± 25
50/50 NR/BG fibrous mat	5.2 ± 0.5	1.17 ± 0.14	290 ± 19

respectively, higher than those of the NR film (0.35 ± 0.05 MPa and 0.98 ± 0.02 MPa, respectively). This increase in the *Y* value of the NR fibrous mat compared to the NR film could be explained using the mechanism of deformation of the fibrous mat based on axial alignment and the formation of beams by the microfibers owing to the imposed tension. Moreover, the adhesion that occurred at the contact points between the microfibers acted as "soldering points" and contributed to this behavior. The soldering points are therefore the result of specific joining points between microfibers due to incomplete drying of the solvent while traveling the working distance to the collector.

The same behavior was observed for the biocomposite samples. The *Y* values of the NR/BG biocomposites were higher and the elongation at break ($\varepsilon_{at\ break}$) values were lower than those of the NR film. The mechanical properties of composites can be influenced by several factors, i.e., the volumetric fractions of phases (filer and matrix), distribution and orientation of fillers in the matrix, filler morphology, aspect ratio (length/diameter), etc. [16]. While the *Y* value of the 90/10 NR/BG fibrous mat was similar to that of the NR fibrous mat, the $\sigma_{at\ break}$ and $\varepsilon_{at\ break}$ values of this fibrous mat were slightly higher than those of the NR fibrous mat. This behavior suggested that the reinforcing properties of the BG particles are effective for loading BG amounts up to 10 wt%.

For higher loads of BG particulates, i.e., the 70/30 and 50/50 fibrous mat biocomposite, a larger number of defects that deteriorated the mechanical properties of the NR matrix appeared more frequently, and as a consequence lower Young modulus, $\sigma_{at\ break}$, and $\varepsilon_{at\ break}$ values of the membranes were observed (Table 1) [10]. Using SEM analysis (Fig. 2) we observed that the amount of BG particles and agglomerate on the surfaces of microfibers increased with the increase in the concentration of BG of the biocomposite. In addition, the BG particle distribution became more heterogeneous. These defects that appeared in the NR microfibers due to high amount of BG filler acted as rupture points (during axial alignment) when the samples were subjected to the action of external mechanical tension, as observed in the SEM images. Although increasing the amount of BG added to the NR microfibers increased the number of BG particles on the surface of the microfibers, it was possible to incorporate up to 50% m/m BG into the NR microfibers without affecting the good mechanical properties of the biocomposites, as illustrated in Table 1.

3.4. Dynamic mechanical thermal analysis (DMTA)

The DMTA method involves applying a stress or strain to a sample and analyzing the response to obtain the phase angle and deformation data, i.e., studying the stress, temperature, and frequency of the material subjected to a small variable mechanical stress [31]. Using these data, it is possible to calculate tan δ, the complex modulus (E' and E'') and viscoelastic parameters of samples. During cyclic strain, the complex storage modulus E^* can be written as:

$$E^* = E^{'} + iE'' \quad (1)$$

where E' is the storage modulus (quantity of energy stored and retained during the load application cycle) and E'' is the loss modulus (energy dissipated during the cycle). In addition, tan δ can be calculated using the equation:

$$\tan\delta = \frac{E^{''}}{E^{'}} \quad (2)$$

Most materials are subjected to dynamic deformations or strain during their life cycles, therefore, it is important to investigate the dynamic mechanical properties of composites materials analyzed using different modes of cyclic deformation and relaxation processes similar to those they will be exposed to [31]. Fig. 4a shows the behavior of E' as a function of temperature for the NR film, NR membrane, and biocomposites. The dynamic mechanical properties of the samples were considerably influenced by the morphological structure and amount of BG particles. At temperatures below T_g, the E' values of the NR fibrous mat were higher than those of the NR film obtained by casting, and this was attributed to the alignment of the microfibers under the action of mechanical stress. In turn, the increase in E' at temperatures below T_g with the increase in the amount of BG particles in the biocomposites is due to the increase in stress transfer to the matrix induced by the BG filler. The increase in E' in the glassy region (plateau) indicates an increase in stiffness and restricted chains movement, inducing higher stored energy in these materials [32,33].

From Fig. 4a we noticed that E' of the 50/50 NR/BG sample was smaller than that of the 70/30 NR/BG sample. This behavior may be due to the larger amount of BG filler mainly on the surface of the microfibers for the 50/50 NR/BG sample. The BG particles would generate a greater number of defects and holes in the fibrous matrix, which would, in turn, act as rupture points, thus leading to the decrease in the energy stored during the deformation cycle. This behavior corroborates with the data obtained from analyzing the mechanical properties observed in the strain-stress curve in Fig. 4.

The value of E' decreased as the temperature increased for all samples, which was attributed to the increase in molecular mobility of the NR chains. Around T_g (between −50 and −28 °C) E' tends to lower values for all samples indicating that little energy was stored at temperatures higher than T_g [33]. Above T_g, increasing the BG concentration also increased the E' value. Contrary to what was observed for $T < T_g$, the E' values for the 50/50 samples were higher than those observed for the 70/30 samples. This fact was attributed to the decrease in NR viscosity, which reduced the influence of the defects.

The viscous response of a material, or its ability to dissipate energy during cyclic deformation, mainly as heat, is represented by E'' [34,35]. Fig. 4b shows E'' as a function of temperature for the different samples studied. As can be seen, incorporating the BG filler caused a broadening of the peak of E''. This behavior may be attributed to the inhibition of the relaxation process of the NR chairs because of adding the BG filler. The increase in the peak value of E'' for biocomposites with higher BG amounts was an interesting observation. Such behavior can be attributed to the increase in internal friction which promoted energy dissipation [36]. On the other hand, the amplification and broadening of

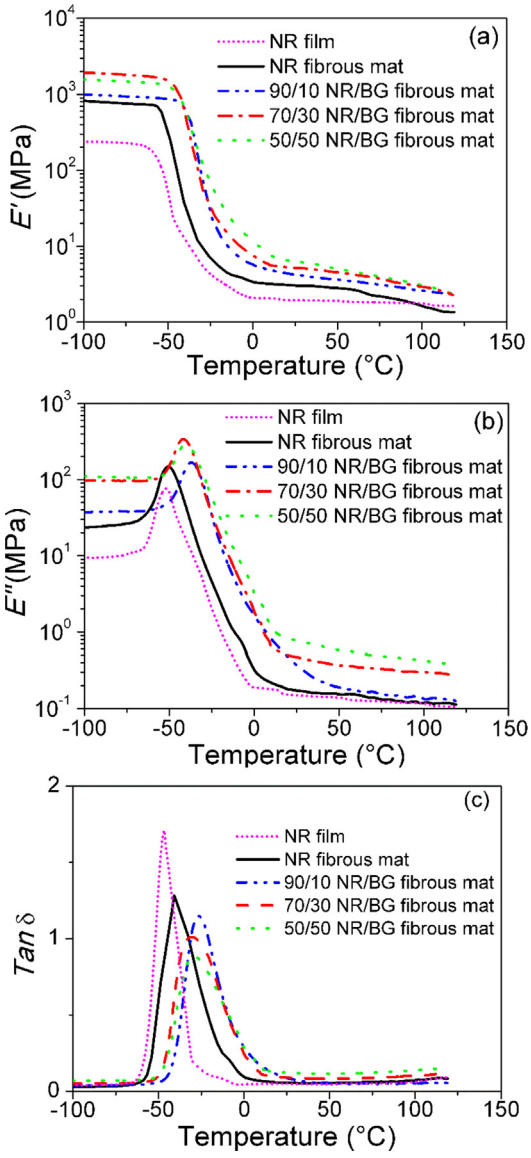

Fig. 4. DMTA of the NR film, NR fibrous mat, and NR/BG fibrous mats biocomposite containing various BG loading amounts. (a) E′, (b) E″, and (c) tan δ as functions of temperature.

Table 2
DMTA parameters: T_{ond}, T_{offd}, T_g and *FWHM* of the samples.

Sample	T_{ond} (°C)	T_{offd} (°C)	T_g (°C)	*FWHM*
NR film	−66.2	−7.5	−46.7	13.1
NR fibrous mat	−60.5	5.5	−40.5	24.5
90/10 NR/BG fibrous mat	−52.5	13.2	−30.4	24.6
70/30 NR/BG fibrous mat	−53.1	11.4	−29.3	27.2
50/50 NR/BG fibrous mat	−53.4	14.2	−29.7	30.7

the peaks of the NR fibrous mat compared to those of the NR films obtained by casting was related to the upsurge in energy dissipation resulting from the movement of the entangled microfibers in the direction of the mechanical stress.

The mechanical loss factor or tan δ represents the damping properties of the material and denotes the equilibrium between the elastic and viscous behavior in the structure of polymeric materials [37,38]. On the other hand, for composites, this behavior is influenced by the type, distribution, and quantity of filler, as well as the interaction of the phases forming the composite [38]. The relaxation process represented

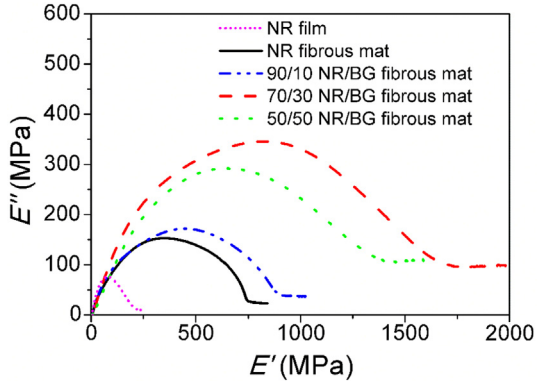

Fig. 5. Cole–Cole diagram of the NR film, NR fibrous mat, and NR/BG fibrous mats biocomposite containing various BG loading amounts.

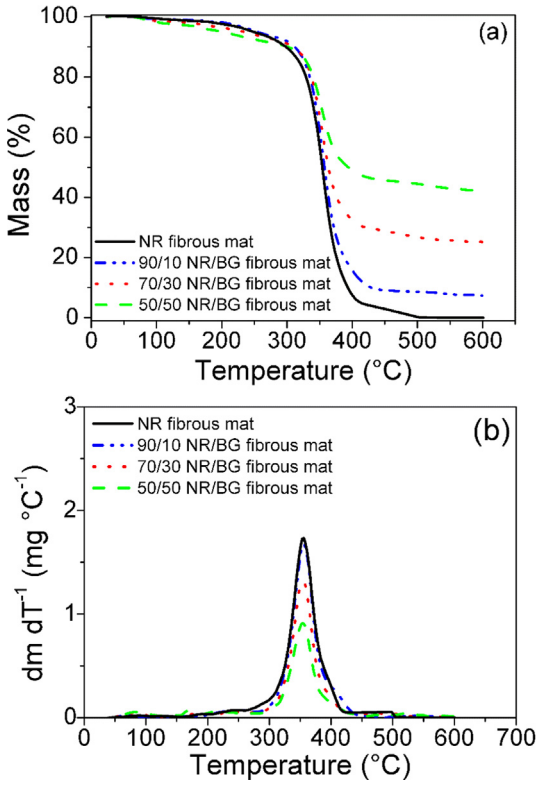

Fig. 6. (a) TG and (b) DTG curves of the NR fibrous mat, and NR/BG fibrous mats biocomposite containing various BG loading amounts.

Table 3
Thermal decomposition parameters: T_{on}, T_m, and residues of the samples.

Sample	T_m (°C)	T_{on} (°C)	Residue (mass%)
NR film	378	332	0.9
NR fibrous mat	356	314	0.5
90/10 NR/BG fibrous mat	355	320	7.5
70/30 NR/BG fibrous mat	353	316	25.7
50/50 NR/BG fibrous mat	343	316	42.3

by the peak of the tan δ versus temperature graph (Fig. 4c) is related to the glass-rubber transition of the NR matrix, i.e., the relaxation process, denoted by α, involved the cooperative motions of polymer chains. Fig. 4c illustrates that the peak value of tan δ decreased as the BG amount in the NR matrix increased. The introduction of fillers into the NR matrix restricted the movement of the polymer chains attributed to polymer adhesion on the BG surface, resulting in higher E' values of the

NR/BG fibrous mat biocomposites compared to those of the NR films and membranes.

The displacement of the peak of tan δ toward higher temperatures was attributed to the introduction of the BG filler into the NR matrix, i.e., the T_g values of the fibrous mat biocomposite increased owing to the BG particles restricting the mobility of the NR chains [32]. The intensity of the peak of tan δ of the NR film was higher than that of the NR fibrous mat and NR/BG biocomposites. This was attributed to the high elasticity of NR film and its greater tendency to dissipate energy during deformation compared to that of the other samples.

Table 2 presents the offset and onset temperatures (T_{offd} and T_{ond} , respectively) and T_g values of all samples. The values of all parameters of the NR fibrous mat were higher than those of the NR film. The T_g value shifted from − 46.7 °C for the NR film to − 40.5 °C for the NR fibrous mat. Moreover, the T_g values of the NR/BG fibrous mat biocomposites ranged between –31 and –28 °C, which were higher than that of the NR fibrous mat. Such behavior indicated that the heat transfer to the membrane samples during testing was delayed owing to the porous structure of the membranes. Moreover, the T_{offd}, T_{ond}, and T_g of the NR/BG biocomposites were higher than those of the NR fibrous mat owing to the mobility of the polymer chains bound to the surface of the biomaterial being restricted.

Another important parameter that can be analyzed in the tan δ graph as a function of temperature is the full width half maximum (*FWHM*) or peak width at half height [39]. This parameter represents the relaxation process in composite materials and tends to increase with an increasing amount of charge [40]. According to Pistor et al. [41], the peak width differs according to the homogeneity of the system, in which a wider width reflects a greater difference in relaxation time, and a narrower peak width denotes a lower difference in the relaxation time of the polymeric chain. The *FWHM* values of all samples obtained from the tan δ graph are presented in Table 2. The highest *FWHM* value was found for the sample with 50% BG, which was expected considering the fact that as the amount of BG filler becomes larger, the relaxation times increase due to NR adhesion on the BG surface.

The Cole-Cole method, originally developed for studying the dielectric behavior of materials, is a good tool to determine changes in the viscoelastic characteristics of polymers and composites materials [42]. This method uses the complex modulus, E^*, where the plot of the loss modulus (E'') versus the storage modulus (E') in a complex plane can be used to estimate the degree of homogeneity of the composite [43]. Homogenous systems are characterized by a semicircle in the Cole–Cole plots, while heterogeneous systems should present imperfect semicircles [35,44]. Fig. 5 illustrates semicircles for the NR film, NR fibrous mat, and fibrous mat biocomposites. The imperfect semicircular shape of the plot indicates the heterogeneity of the system and adequate interaction between the BG particles and NR microfibers. As the BG filler content increased, the semicircle became larger indicating that the NR matrix became stiffer.

3.5. TG/DTG analysis

Fig. 6 shows the thermogravimetry (TG)/differential thermogravimetry (DTG) curves of the NR and fibrous mat biocomposites. The mass loss in the 25–300 °C range for all samples was attributed to water evaporation (below 120 °C) and the decomposition of non-rubber components, e.g., fatty acids (in the 150–300 °C range) [45]. The estimated mass loss due to these two processes was approximately 10%. The TG profile of the NR fibrous mat and NR/BG fibrous mat biocomposites basically displayed one main weight loss event in the 300–450 °C temperature range (Fig. 6a). This event appears as the most intense peak in Fig. 6b and was attributed to the structural decomposition of the NR chains [13,45]. The mass loss corresponding to this event was approximately 90% for the NR mat and 82, 60, and 41.5% for the 90/10, 70/30, and 50/50 biocomposites samples, respectively. These values were approximately equal to the amounts of NR in the biocomposite. The thermal stability did not change with the addition of BG particles to the biocomposite compared to the NR fibrous mat.

Table 3 summarizes the thermal decomposition parameters, such as the temperature at the maximum decomposition rate (T_m), onset temperature (T_{on}), and offset temperature (T_{off}) of the intense peak and the residues of the samples at 600 °C. Small variations in T_m, T_{on}, and T_{off} of all samples studied can be observed. On the other hand, the residues at 600 °C were larger for the samples containing greater amounts of BG filler. The calculated values were very close to the BG amounts used to obtain the biocomposites.

4. Conclusion

A NR fibrous mat and NR/BG fibrous mat biocomposite containing different amounts of BG fillers were obtained using SBS. The samples exhibited ribbon-like morphology, and the width of their microfibers was in the range of 40–60 μm. The SEM and optical images indicated the good distribution of the BG particles present on the surface of and inside the NR microfibers. The stress–strain tests demonstrated that the Y and $\sigma_{at\ break}$ values of the NR fibrous mat were substantially higher (6.12 ± 0.09 MPa and 1.62 ± 0.12 MPa, respectively) than those of the NR film (0.35 ± 0.05 MPa and 0.98 ± 0.02 MPa, respectively). Moreover, even when large amounts of BG were incorporated into the NR matrix, Y and $\sigma_{at\ break}$ of the NR/BG biocomposites were superior to those of NR film. The Y, $\sigma_{at\ break}$, and $\varepsilon_{at\ break}$ of the 50/50 NR/BG fibrous mat biocomposite were 5.2 ± 0.5 MPa, 1.17 ± 0.14 MPa, and 290 ± 19%, respectively. The T_g values of the NR film and NR fibrous mat were approximately − 46.7 and − 40.5 °C, respectively, and those of the fibrous mat biocomposites were in the range of –31 to –28 °C. Such behavior was attributed to the stretching of the NR during processing combined with the BG particles restricting the mobility of the NR chains. The results of the TG analysis demonstrated that the neat NR and NR/BG biocomposites exhibited similar thermal profiles, and presented good thermal stability up to ~ 200 °C. The results above demonstrated that SBS could be used as an alternative technique to produce biocomposites with potential biomedical applications.

Acknowledgments

The authors would like to thank the Coordenação de Aperfeiçoamento de Pessoal de Nível Superior (CAPES) and Conselho Nacional de Desenvolvimento Científico e Tecnológico (CNPq) for the financial support and awarded scholarship.

References

[1] O.O. Ige, L.E. Umoru, S. Aribo, Natural products: a minefield of biomaterials, ISRN Mater. Sci. 2012 (2012) 1–20, https://doi.org/10.5402/2012/983062.
[2] J.E. Gough, A.R. Boccaccini, Tissue Engineering Using Ceramics and Polymers, 2007. 10.1533/9781845693817.
[3] R.L. Siqueira, E.D. Zanotto, Biosilicate®: historical of a highly bioactive brazilian glass-ceramic, Quim. Nova. 34 (2011) 1231–1241, https://doi.org/10.1590/S0100-40422011000700023.
[4] J. Moura, L.N. Teixeira, C. Ravagnani, O. Peitl, E.D. Zanotto, M.M. Beloti, H. Panzeri, A.L. Rosa, P.T. De Oliveira, In vitro osteogenesis on a highly bioactive glass-ceramic (Biosilicate®), J. Biomed. Mater. Res. - Part A. 82 (2007) 545–557, https://doi.org/10.1002/jbm.a.31165.
[5] L.L. Hench, The story of Bioglass®, J. Mater. Sci. Mater. Med. (2006) 967–978, https://doi.org/10.1007/s10856-006-0432-z.
[6] V. Krishnan, T. Lakshmi, Bioglass: a novel biocompatible innovation, J. Adv. Pharm. Technol. Res. 4 (2013) 78, https://doi.org/10.4103/2231-4040.111523.
[7] S. Hu, J. Chang, M. Liu, C. Ning, Study on antibacterial effect of 45S5 Bioglass®, J. Mater. Sci. Mater. Med. 20 (2009) 281–286, https://doi.org/10.1007/s10856-008-3564-5.
[8] A.O. Paiva, M.G. Duarte, M.H.V. Fernandes, M.H. Gil, N.G. Costa, In Vitro studies of bioactive glass/polyhydroxybutyrate composites, Mater. Res. 9 (2006) 417–423, https://doi.org/10.1590/S1516-14392006000400013.
[9] L.-C. Gerhardt, A.R. Boccaccini, Bioactive glass and glass-ceramic scaffolds for bone tissue engineering, Materials (Basel) 3 (2010) 3867–3910, https://doi.org/10.3390/ma3073867.
[10] N. Liao, M.K. Joshi, A.P. Tiwari, C.H. Park, C.S. Kim, Fabrication, characterization

and biomedical application of two-nozzle electrospun polycaprolactone/zein-calcium lactate composite nonwoven mat, J. Mech. Behav. Biomed. Mater. (2016), https://doi.org/10.1016/j.jmbbm.2016.02.006.
[11] M.J. Silva, V.O. Soares, G.C. Dias, R.J. Santos, A.E. Job, A.O. Sanches, J.A. Malmonge, Study of thermal and mechanical properties of a biocomposite based on natural rubber and 45S5 Bioglass® particles, J. Therm. Anal. Calorim. 131 (2018), https://doi.org/10.1007/s10973-016-5933-5.
[12] L. Huang, J. Tan, W. Li, L. Zhou, Z. Liu, B. Luo, L. Lu, C. Zhou, Functional polyhedral oligomeric silsesquioxane reinforced poly(lactic acid) nanocomposites for biomedical applications, J. Mech. Behav. Biomed. Mater. 90 (2019) 604–614, https://doi.org/10.1016/j.jmbbm.2018.11.002.
[13] E.S. Medeiros, P.D. Galiani, R.M.B. Moreno, L.H.C. Mattoso, J.A. Malmonge, A comparative study of the non-isothermal degradation of natural rubber from Mangabeira (Hancornia speciosa Gomes) and Seringueira (Hevea brasiliensis), in: J. Therm. Anal. Calorim., 2010: pp. 1045–1050. 10.1007/s10973-009-0477-6.
[14] J.F.F., F.C.N., L.S.L.S. da M., E.L.F., R.S.F., B.B., P.J.G., L.M. de A., F.A.B., R. Graeff, Comparative study of bone tissue accelerated regeneration by latex membranes from Hevea brasiliensis and Hancornia speciosa, Biomed. Phys. Eng. Exp. 2 (2016) 45007. 10.1088/2057-1976/2/4/045007.
[15] N.R. De Barros, P.A.M. Chagas, F.A. Borges, J.L.P. Gemeinder, M.C.R. Miranda, B.C. Garms, R.D. Herculano, Diclofenac potassium transdermal patches using natural rubber latex biomembranes as carrier, J. Mater. 2015 (2015) 1–7, https://doi.org/10.1155/2015/807948.
[16] H.A. Metwally, R.V. Ardazishvili, A.N. Severyukhina, A.M. Zaharevich, A.A. Skaptsov, S.B. Venig, G.B. Sukhorukov, D.A. Gorin, The influence of hydroxyapatite and calcium carbonate microparticles on the mechanical properties of nonwoven composite materials based on polycaprolactone, Bionanoscience 5 (2014) 22–30, https://doi.org/10.1007/s12668-014-0158-1.
[17] H. Mi, X. Jing, E. Yu, X. Wang, Q. Li, L. Turng, Manipulating the structure and mechanical properties of thermoplastic polyurethane/polycaprolactone hybrid small diameter vascular sca ff olds fabricated via electrospinning using an assembled rotating collector, J. Mech. Behav. Biomed. Mater. 78 (2018) 433–441, https://doi.org/10.1016/j.jmbbm.2017.11.046.
[18] G. Tetteh, A.S. Khan, R.M. Delaine-Smith, G.C. Reilly, I.U. Rehman, Electrospun polyurethane/hydroxyapatite bioactive Scaffolds for bone tissue engineering: the role of solvent and hydroxyapatite particles, J. Mech. Behav. Biomed. Mater. (2014), https://doi.org/10.1016/j.jmbbm.2014.06.019.
[19] A. Podshivalov, M. Zakharova, E. Glazacheva, M. Uspenskaya, Gelatin/potato starch edible biocomposite films: correlation between morphology and physical properties, Carbohydr. Polym. 157 (2017) 1162–1172, https://doi.org/10.1016/j.carbpol.2016.10.079.
[20] K.A. Iyer, J.M. Torkelson, Dispersion and property enhancements in polyolefin/soy flour biocomposites prepared via melt extrusion followed by solid-state shear pulverization, Macromol. Mater. Eng. 300 (2015) 772–784, https://doi.org/10.1002/mame.201500019.
[21] J.L. Daristotle, A.M. Behrens, A.D. Sandler, P. Kofinas, A review of the fundamental principles and applications of solution blow spinning, ACS Appl. Mater. Interfaces. 8 (2016) 34951–34963, https://doi.org/10.1021/acsami.6b12994.
[22] C.R. Cena, M.J. Silva, L.F. Malmonge, J.A. Malmonge, Poly(vinyl pyrrolidone) submicrofibers produced by solution blow spinning, J. Polym. Res. 25 (2018) 238, https://doi.org/10.1007/s10965-018-1633-0.
[23] E.S. Medeiros, G.M. Glenn, A.P. Klamczynski, W.J. Orts, L.H.C. Mattoso, Solution blow spinning: a new method to produce micro- and nanofibers from polymer solutions, J. Appl. Polym. Sci. 113 (2009) 2322–2330, https://doi.org/10.1002/app.30275.
[24] C.R. Cena, A.K. Behera, B. Behera, Structural, dielectric, and electrical properties of lithium niobate microfibers, J. Adv. Ceram. 5 (2016), https://doi.org/10.1007/s40145-015-0176-7.
[25] E.L.G. Medeiros, A.L. Braz, I.J. Porto, A. Menner, A. Bismarck, A.R. Boccaccini, W.C. Lepry, S.N. Nazhat, E.S. Medeiros, J.J. Blaker, Porous bioactive nanofibers via cryogenic solution blow spinning and their formation into 3D macroporous scaffolds, ACS Biomater. Sci. Eng. (2016), https://doi.org/10.1021/acsbiomaterials.6b00072.
[26] Y.J. Dias, T.C. Gimenes, S.A.P.V. Torres, J.A. Malmonge, A.J. Gualdi, F.R. de Paula, PVDF/Ni fibers synthesis by solution blow spinning technique, J. Mater. Sci. Mater. Electron. 29 (2018) 514–518, https://doi.org/10.1007/s10854-017-7941-z.
[27] S. Koombhongse, W. Liu, D.H. Reneker, Flat polymer ribbons and other shapes by electrospinning, J. Polym. Sci. Part B Polym. Phys. (2001), https://doi.org/10.1002/polb.10015.
[28] A. Koski, K. Yim, S. Shivkumar, Effect of molecular weight on fibrous PVA produced by electrospinning, Mater. Lett. (2004), https://doi.org/10.1016/S0167-577X(03)00532-9.
[29] C.L. Casper, J.S. Stephens, N.G. Tassi, D.B. Chase, J.F. Rabolt, Controlling surface morphology of electrospun polystyrene fibers: effect of humidity and molecular weight in the electrospinning process, Macromolecules (2004), https://doi.org/10.1021/ma0351975.
[30] M. Dhanalakshmi, J.P. Jog, Preparation and characterization of electrospun fibers of Nylon 11, Exp. Polym. Lett. (2008), https://doi.org/10.3144/expresspolymlett.2008.65.
[31] K.P. Menard, N.R. Menard, Dynamic Mechanical Analysis in the Analysis of Polymers and Rubbers, 2015. 10.1002/0471440264.pst102.pub2.
[32] H. Rajashekaraiah, S. Mohan, P.K. Pallathadka, S. Bhimappa, Dynamic mechanical analysis and three-body abrasive wear behaviour of thermoplastic copolyester elastomer composites, Adv. Tribol. 2014 (2014), https://doi.org/10.1155/2014/210187.
[33] M. Bhattacharya, A.K. Bhowmick, Synergy in carbon black-filled Natural rubber nanocomposites. Part I: mechanical, dynamic mechanical properties, and morphology, J. Mater. Sci. 45 (2010) 6126–6138, https://doi.org/10.1007/s10853-010-4699-6.
[34] H.L. Ornaghi, A.S. Bolner, R. Fiorio, A.J. Zattera, S.C. Amico, Mechanical and dynamic mechanical analysis of hybrid composites molded by resin transfer molding, J. Appl. Polym. Sci. 118 (2010) 887–896, https://doi.org/10.1002/app.32388.
[35] M. Jawaid, H.P.S.A. Khalil, Effect of layering pattern on the dynamic mechanical properties and thermal degradation of oil palm-jute fibers reinforced epoxy hybrid composite, BioResources 6 (2011) 2309–2322.
[36] N. Saba, M. Jawaid, O.Y. Alothman, M.T. Paridah, A review on dynamic mechanical properties of natural fibre reinforced polymer composites, Constr. Build. Mater. 106 (2016) 149–159, https://doi.org/10.1016/j.conbuildmat.2015.12.075.
[37] S. Manoharan, B. Suresha, G. Ramadoss, B. Bharath, Effect of Short Fiber Reinforcement on Mechanical Properties of Hybrid Phenolic Composites, Article ID, 2014, pp. 5–11.
[38] K. Jayanarayanan, S. Thomas, K. Joseph, Morphology, static and dynamic mechanical properties of in situ microfibrillar composites based on polypropylene/poly (ethylene terephthalate) blends, Compos. Part A Appl. Sci. Manuf. 39 (2008) 164–175, https://doi.org/10.1016/j.compositesa.2007.11.008.
[39] X. Fernández-Francos, X. Ramis, Structural analysis of the curing of epoxy thermosets crosslinked with hyperbranched poly(ethyleneimine)s, Eur. Polym. J. (2015), https://doi.org/10.1016/j.eurpolymj.2015.07.031.
[40] D. Romanzini, H.L. Ornaghi, S.C. Amico, A.J. Zattera, Influence of fiber hybridization on the dynamic mechanical properties of glass/ramie fiber-reinforced polyester composites, J. Reinf. Plast. Compos. (2012), https://doi.org/10.1177/0731684412459982.
[41] V. Pistor, F.G. Ornaghi, H.L. Ornaghi, A.J. Zattera, Dynamic mechanical characterization of epoxy/epoxycyclohexyl-POSS nanocomposites, Mater. Sci. Eng. A. (2012), https://doi.org/10.1016/j.msea.2011.10.100.
[42] C.S.M.F. Costa, A.C. Fonseca, A.C. Serra, J.F.J. Coelho, Dynamic mechanical thermal analysis of polymer composites reinforced with natural fibers, Polym. Rev. 56 (2016) 362–383, https://doi.org/10.1080/15583724.2015.1108334.
[43] M.H. Gheith, M.A. Aziz, W. Ghori, N. Saba, M. Asim, M. Jawaid, O.Y. Alothman, Flexural, thermal and dynamic mechanical properties of date palm fibres reinforced epoxy composites, J. Mater. Res. Technol. 8 (2019) 853–860, https://doi.org/10.1016/j.jmrt.2018.06.013.
[44] Y. Karaduman, M.M.A. Sayeed, L. Onal, A. Rawal, Viscoelastic properties of surface modified jute fiber/polypropylene nonwoven composites, Compos. Part B Eng. (2014), https://doi.org/10.1016/j.compositesb.2014.06.019.
[45] D.L.S. Agostini, C.J.L. Constantino, A.E. Job, Thermal degradation of both latex and latex cast combined TG/FTIR investigation, J. Therm. Anal. Calorim. 91 (2008) 703–707.